Published in final edited form as:

J Am Chem Soc. 2017 September 27; 139(38): 13541–13553. doi:10.1021/jacs.7b07612.

A Diaminopropane-Appended Metal–Organic Framework Enabling Efficient CO_2 Capture from Coal Flue Gas via a Mixed Adsorption Mechanism

Phillip J. Milner[†], **Rebecca L. Siegelman**[†], **Alexander C. Forse**[†,‡], **Miguel I. Gonzalez**[†], **Tomče Runčevski**[†,§], **Jeffrey D. Martell**[†], **Jeffrey A. Reimer**[#], **Jeffrey R. Long**[*,†,#,§]

[†]Department of Chemistry, University of California, Berkeley, California 94720, United States

[‡]Berkeley Energy and Climate Institute, University of California, Berkeley, California 94720, United States

[#]Department of Chemical and Biomolecular Engineering, University of California, Berkeley, California 94720, United States

[§]Materials Sciences Division, Lawrence Berkeley National Laboratory, Berkeley, California 94720, United States

Abstract

A new diamine-functionalized metal–organic framework comprised of 2,2-dimethyl-1,3-diaminopropane (dmpn) appended to the Mg^{2+} sites lining the channels of Mg_2(dobpdc) (dobpdc^{4-} = 4,4′-dioxido-3,3′-biphenyldicarboxylate) is characterized for the removal of CO_2 from the flue gas emissions of coal-fired power plants. Unique to members of this promising class of adsorbents, dmpn–Mg_2(dobpdc) displays facile step-shaped adsorption of CO_2 from coal flue gas at 40 °C and near complete CO_2 desorption upon heating to 100 °C, enabling a high CO_2 working capacity (2.42 mmol/g, 9.1 wt%) with a modest 60 °C temperature swing. Evaluation of the thermodynamic parameters of adsorption for dmpn–Mg_2(dobpdc) suggests that the narrow temperature swing of its CO_2 adsorption steps is due to the high magnitude of its differential enthalpy of adsorption (Δh_{ads} = −73 ± 1 kJ/mol), with a larger than expected entropic penalty for CO_2 adsorption (Δs_{ads} = −204 ± 4 J/mol·K) positioning the step in the optimal range for carbon capture from coal flue gas. In addition, thermogravimetric analysis and breakthrough experiments indicate that, in contrast to many adsorbents, dmpn–Mg_2(dobpdc) captures CO_2 effectively in the presence of water and can be subjected to 1000 humid adsorption/desorption cycles with minimal degradation. Solid-state ^{13}C NMR spectra and single-crystal X-ray diffraction structures of the Zn analogue reveal that this material adsorbs CO_2 via formation of both ammonium carbamates and

[*]**Corresponding Author** jrlong@berkeley.edu.

ASSOCIATED CONTENT

Full characterization of all new adsorbents and additional experimental details are included in the Supporting Information. The .cif files for Zn_2(dobpdc)(dmen)$_{1.61}$·(H_2O)$_{0.70}$, Zn_2(dobpdc)(dmen)$_{0.98}$(dmen–CO_2)$_{0.76}$, Zn_2(dobpdc)(mpn)$_{1.76}$(C_7H_8)$_{0.62}$, Zn_2(dobpdc)(dmpn)$_{1.3}$, and Zn_2(dobpdc)(dmpn)$_{0.65}$(dmpn–CO_2)$_{0.77}$ are included as well.

The authors declare the following competing financial interest: J.R.L. has a financial interest in Mosaic Materials, Inc., a start-up company working to commercialize metal–organic frameworks for gas separations, including CO_2 capture applications. The University of California, Berkeley has applied for a patent on some of the materials discussed herein, on which J.R.L., P.J.M., and R.L.S. are listed as inventors.

carbamic acid pairs, the latter of which are crystallographically verified for the first time in a porous material. Taken together, these properties render dmpn–Mg_2(dobpdc) one of the most promising adsorbents for carbon capture applications.

Graphical Abstract

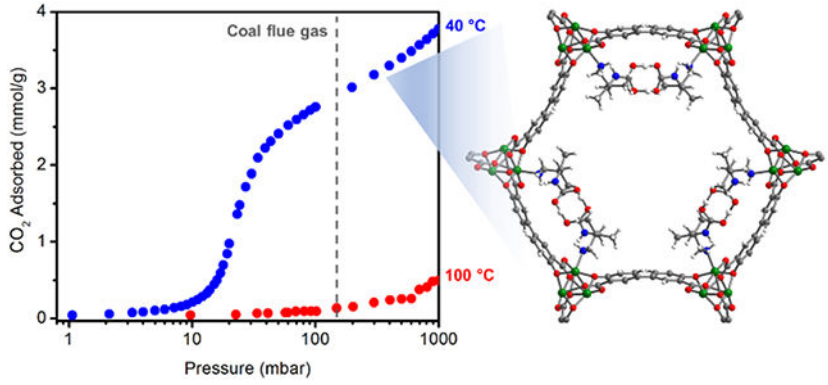

INTRODUCTION

Rising atmospheric levels of greenhouse gases, primarily CO_2, are linked to global climate change.[1] In particular, the combustion of coal for energy generation accounts for approximately 30% of global CO_2 emissions.[2] Despite this, coal is projected to remain a major energy source in the near future, especially in rapidly industrializing nations.[2,3] Therefore, post-combustion carbon capture and sequestration (CCS) from coal flue gas, which consists of CO_2 (15–16%), O_2 (3–4%), H_2O (5–7%), N_2 (70–75%), and trace impurities (e.g. SO_x, NO_x) at ambient pressure,[4] is a key strategy needed to reduce global CO_2 emissions during the transition to cleaner energy sources.[1,5] Because 60–70% of the cost of CCS is accrued during the CO_2 separation stage, the development of improved adsorbents for carbon capture stands to limit substantially the rise in cost of electricity upon implementation of CCS.[6] Specifically, a temperature swing adsorption (TSA) process requires an adsorbent that: (i) selectively adsorbs CO_2 under typical coal flue gas conditions (150 mbar of CO_2 at 40 °C), (ii) captures 90% of the CO_2 from the stream, (iii) is regenerable at low temperatures under pure CO_2 to minimize regeneration costs, (iv) displays fast adsorption/desorption kinetics, and (v) possesses long-term stability to both water and adsorption/desorption cycling.[6b,7]

The most widely employed sorbents for CCS are aqueous solutions of organic amines, such as monoethanolamine (MEA), which selectively react with CO_2 to form ammonium carbamate and/or bicarbonate species.[6a,8] However, amine solutions are prone to oxidative and thermal degradation[8a,9] and suffer from low CO_2 working capacities, contributing to an untenable increase in the cost of electricity if employed for CCS.[6,10] To address these issues, solid adsorbents, including porous carbons, silicas, zeolites, and metal–organic frameworks, have been investigated as promising alternatives due to their high thermal stabilities and potentially lower regeneration energies.[5a,7,11] Extensive studies have revealed that most of these adsorbents are not applicable for CCS due to hydrolytic instability and/or competitive

binding of water to the CO_2 adsorption sites.[11a,c-g,12,13] On the other hand, amine-functionalized adsorbents[11b,d,f,g,14] can offer both high CO_2 selectivity and enhanced performance under humid conditions,[12b,14b,15] but often exhibit slow adsorption kinetics[12b] and require high regeneration temperatures. Thus, there remains an ongoing need for new adsorbents that perform well under humid conditions and can be regenerated at moderate temperatures under pure CO_2.

Recently, we[16] and others[17] have investigated a new class of amine-functionalized adsorbents prepared by appending diamines to the open metal sites of metal–organic frameworks. Remarkably, alkylethylenediamine-appended variants of Mg_2(dobpdc) (dobpdc^{4-} = 4,4′-dioxidobiphenyl-3,3′-dicarboxylate),[16a-c,17a-c] a metal–organic framework possessing hexagonal one-dimensional channels lined with coordinatively-unsaturated Mg^{2+} sites, adsorb CO_2 via a unique cooperative mechanism involving the formation of ammonium carbamate chains (Figure 1).[16a,b] This cooperative adsorption leads to step-shaped isotherms that enable high working capacities in a TSA process (Figure 2).[16a,b] In addition, previous mixed-gas equilibrium adsorption measurements indicate that these materials maintain their high capacity for CO_2 under humid conditions, a critical challenge for carbon capture.[12b,16b,17a]

Owing to their highly exothermic differential enthalpies of adsorption, Mg_2(dobpdc) variants appended with *primary,secondary* (1°,2°),[16a] *secondary,secondary* (2°,2°),[16a-c] and most *primary,primary* (1°,1°)[17a,c] alkylethylenediamines display step-shaped adsorption of CO_2 at very low partial pressures (≤1 mbar of CO_2 at 40 °C) (Figure 2). As a result of their low step pressures, these adsorbents are well-suited for carbon capture from dilute streams such as air.[16a,c,17c] However, this strong adsorption results in high desorption temperatures under pure CO_2 (140–200 °C), which greatly increases the regeneration costs associated with the use of these adsorbents. In contrast, *primary,tertiary* (1°,3°) diamine-appended variants of Mg_2(dobpdc) can be regenerated at lower temperatures (75 °C), but due to their relatively high step pressures (≥ 100 mbar, 40 °C) would capture only ≤ 30% of the CO_2 from a coal flue gas stream (Figure 2).[16a,17b] A promising adsorbent would display step-shaped adsorption at ~15 mbar of CO_2 at 40 °C to enable 90% capture from a coal flue gas stream containing 150 mbar of CO_2, and minimal adsorption under 1 bar of CO_2 at ≤ 100 °C to enable regeneration of the CO_2-saturated bed with lower grade steam. More specifically, the ideal adsorbent would possess a free energy of adsorption (Δg_{ads}) as close as possible to that required for a CO_2 adsorption step (p_{step}) at 15 mbar at 40 °C (−10.9 kJ/mol, as determined from $\Delta g_{ads} = RT\ln(p_{step}/p_0)$ with p_0 = 1 bar),[16a] which will enable effective capture of CO_2 while minimizing the energy required for desorption. None of the alkylethylenediamine-appended variants of Mg_2(dobpdc) reported to date meet these criteria.[16a-c,17a-c] Herein, we demonstrate that Mg_2(dobpdc) appended with 2,2-dimethyl-1,3-diaminopropane (dmpn, Figure 2) possesses these desirable attributes, while maintaining excellent long-term stability and performance under humid conditions. Altogether, these characteristics make dmpn–Mg_2(dobpdc) one of the most promising adsorbents identified to date for CCS from coal flue gas.

EXPERIMENTAL SECTION

General Procedures.

All synthetic manipulations were carried out under air unless noted otherwise. All diamines and solvents were purchased from commercial sources and used without further purification. The ligand H_4dobpdc was purchased from Hangzhou Trylead Chemical Technology Co. The metal–organic frameworks M_2(dobpdc) (M = Mg, Mn, Co, Ni, Zn) were prepared according to modified literature procedures, as detailed in the Supporting Information.[16a,b] Powder X-ray diffraction patterns (Figure S1) and 77K N_2 adsorption isotherms (Figure S2) for these materials are consistent with those from the literature.[16a,b] ^{1}H NMR spectra for digestion experiments were collected on a Bruker AMX 300 MHz NMR spectrometer and referenced to residual DMSO (δ 2.50 ppm). Attenuated total reflectance (ATR) infrared (IR) spectra were collected on a Perkin-Elmer Spectrum 400 Fourier Transform (FT) IR spectrometer. Differential scanning calorimetry (DSC) measurements were carried out using a TA Instruments Q200 differential scanning calorimeter. Laboratory powder X-ray diffraction patterns were collected using a Bruker AXS D8 Advance diffractometer using Cu$K\alpha$ radiation (λ = 1.5418 Å).

Synthesis of Diamine-Appended M_2(dobpdc) (M = Mg, Ni) Compounds.[16a]

A 20 mL scintillation vial was charged with 4 mL of toluene and 1 mL of the diamine (for 2,2-dimethyl-1,3-diaminopropane, the diamine was melted prior to use). Methanol-solvated M_2(dobpdc) (~20 mg, M = Mg or Ni) was filtered and washed with successive aliquots of toluene (2 × 10 mL) (Note: M_2(dobpdc) should not be allowed to dry completely as this can in some cases lead to decomposition of the framework).[16c] Next, M_2(dobpdc) was added to the diamine solution, and the vial was swirled several times and allowed to stand at room temperature for 24 h. The mixture was then filtered, and the resulting powder was thoroughly washed with toluene (3 × 20 mL) and allowed to dry for 2 min, yielding ~30 mg of the diamine-appended metal–organic framework. In all cases, ^{1}H NMR digestion experiments (Supporting Information Section S5) confirmed that the ratios of diamine to Mg^{2+} sites were >100% (Table S2), indicative of solvation by excess diamine. Activation of the samples at 130–150 °C for 20–30 min under flowing N_2 was sufficient to remove the excess diamine from the pores. A modified procedure[15b] was used to prepare small-scale samples of dmpn–appended M_2(dobpdc) (M = Mn, Co, Zn) (see Supporting Information for details). Powder X-ray diffraction patterns, infrared spectra, pure CO_2 adsorption/desorption isobars, and thermogravimetric N_2 decomposition curves for all new diamine-appended metal–organic frameworks prepared in this work are included in Sections 2-4 of the Supporting Information.

Single-Crystal and Powder X-ray Diffraction Structures.

Details of powder X-ray diffraction refinements are included in Supporting Information Section 10. Single crystals of Zn_2(dobpdc) and diamine-appended analogues were prepared according to modified literature procedures.[16a] Additional details and structures are included in Supporting Information Section 11.

Gas Adsorption Measurements.

Adsorption isotherms of N_2, O_2, CO_2, and H_2O were obtained by volumetric methods using a Micromeritics ASAP 2020 gas adsorption analyzer. All gases were 99.998% purity or higher. Deionized water was subjected to three freeze–pump–thaw cycles prior to adsorption measurements. Isotherms conducted at 25, 30, 40, 50, 60, and 75 °C were measured using a circulating water bath. Isotherms at 100 °C were measured using a heated sand bath equipped with a programmable temperature controller. Samples were regenerated at 100 °C under dynamic vacuum (<10 μbar) for 2–4 h between isotherms. The isotherm data points were considered equilibrated after <0.01% pressure change occurred over a 15 s interval.

Calculations of Differential Enthalpies and Entropies of Adsorption.

Isotherms were fit by linear interpolation. Using the isotherm fits, the exact pressures (p_q) corresponding to specific CO_2 loadings (q) were determined at different temperatures (T). The Clausius–Clapeyron relationship (eq. 1) was used to calculate the differential enthalpies of adsorption (Δh_{ads}) based on the slopes of the linear trendlines fit to $\ln(p_q)$ vs. $1/T$ at constant values of q. The y-intercepts of these linear trendlines are equal to $-\Delta s_{ads}/R$ at each loading (with $p_0 = 1$ bar),[18] and thus were used to determine the corresponding differential entropies of adsorption.

$$\ln(p_q) = \left(\frac{\Delta h_{ada}}{R}\right)\left(\frac{1}{T}\right) + c \quad (1)$$

Thermogravimetric Analysis and Cycling Measurements.

Dry thermogravimetric analysis (TGA) experiments were conducted using a TA Instruments TGA Q5000. Humid TGA experiments were conducted using a TA Instruments TGA Q50. The incident gas stream was humidified by passing it through two water bubblers in series, leading to an estimated water content of 1.3% at 25 °C (as determined by comparison to water isotherms). Isobars were measured using a temperature ramp rate of 1 °C/min. Custom CO_2/N_2 blends (50%, 30%, 15%, 10%, and 5% CO_2 in N_2) were purchased from Praxair. Samples were activated at 130 °C or 150 °C under flowing N_2 for 20–30 min (until the mass stabilized) prior to switching the gas stream. Masses are uncorrected for buoyancy effects. Decomposition experiments were carried out under dry N_2 using a temperature ramp rate of 1.5 °C/min.

Breakthrough Measurements.

See Supporting Information Section 7 for complete experimental details.

Solid-State Magic Angle Spinning (MAS) ^{13}C NMR Experiments.

For NMR experiments performed on samples dosed with $^{13}CO_2$ (Sigma Aldrich, 99 atom % ^{13}C, <3 atom % ^{18}O), samples were first activated under flowing N_2 at the temperatures indicated in Table S2 for 30 min, cooled to room temperature, and transferred to a N_2-filled glovebag. The samples were then packed into rotors. Uncapped rotors were then evacuated for at least 30 min inside a home-built gas-dosing manifold before dosing with $^{13}CO_2$, after

which the samples were allowed to equilibrate for 30 min (see Supporting Information Section 8 for further details). All NMR spectra were recorded at 7.1 T using a DOTY magic angle spinning probe with a 4 mm silicon nitride rotor. A Tecmag Discovery spectrometer capable of double resonance experiments was used. ^{13}C NMR spectra were acquired by cross-polarization from ^{1}H with a contact time of 1 ms, and with continuous-wave ^{1}H decoupling during the acquisition period. All ^{13}C NMR spectra were referenced using the tertiary carbon atom of adamantine with a chemical shift of 38.5 ppm (secondary reference). Sample dosing and NMR experiments were carried out at ambient temperature.

RESULTS AND DISCUSSION

Discovery and Evaluation of dmpn–Mg_2(dobpdc).

Our previous work demonstrated that modifying the nitrogen substituents of diamines allows for rational tuning of the CO_2 step pressure for alkylethylenediamine-appended variants of Mg_2(dobpdc).[16a] However, as summarized in Figure 2, changing the substitution patterns on the nitrogen atoms led to step pressures that were either too high (≥ 100 mbar) or too low (≤ 1 mbar) for the efficient removal of CO_2 from coal flue gas. Therefore, we examined whether changing the substituents on the backbone of the diamine — specifically, switching from ethylenediamines to diaminopropanes — could tune the step pressure to ~15 mbar at 40 °C. To this end, we appended 1,3-diaminopropane (pn, Figure 3) to Mg_2(dobpdc), which produced an adsorbent displaying step-shaped adsorption of CO_2 with a similar step pressure (~0.5 mbar, 40 °C) as compared to other strongly adsorbing diamine-appended variants of Mg_2(dobpdc) (Figure 3a).[16a-c,17a,c] However, in distinct contrast to variants of Mg_2(dobpdc) functionalized with *primary,primary* ethylenediamines (Figure S21),[17a,c] pn–Mg_2(dobpdc) displays almost no hysteresis upon CO_2 desorption, allowing for its near complete regeneration at 130 °C under pure CO_2 (Figure 3b). The addition of a methyl group (2-methyl-1,3-diaminopropane, mpn) to the diamine backbone does not have a significant effect on the CO_2 adsorption step pressure or temperature compared to pn–Mg_2(dobpdc) (Figure 3).

Unexpectedly, with the addition of a second methyl group to the diamine backbone, 2,2-dimethyl-1,3-diaminopropane (dmpn) led to a drastic change in the adsorption properties (Figure 3). For this adsorbent, the CO_2 adsorption step at 40 °C is broadened and shifted to a pressure of ~15 mbar, which is suitable for ~90% capture of CO_2 from coal flue gas (Figure 3a). In addition, near-complete CO_2 desorption can be achieved at 95 °C under pure CO_2 (Figure 3b), although an unusual hysteresis profile is apparent during desorption. This low CO_2 desorption temperature is particularly advantageous because the regeneration temperature of the adsorbent strongly affects the efficiency of a carbon capture process.[19] During the preparation of this manuscript, a similar substituent effect was disclosed for ethylenediamine-appended variants of Mg_2(dobpdc).[17a] Although the adsorbent functionalized with the ethylenediamine analogue of dmpn, 1,1-dimethyl-1,2-ethylenediamine (den, referred to herein as dmen), displays a similar pure CO_2 adsorption step temperature, it possesses a lower CO_2 capacity and a higher CO_2 desorption temperature of 116 °C due to significant hysteresis (see Supporting Information Section 3 for details).[17a]

The ability of dmpn–Mg_2(dobpdc) to effectively capture CO_2 at 40 °C while showing minimal adsorption under 1 bar CO_2 at 95 °C led us to further examine its potential for carbon capture from coal flue gas. Accordingly, CO_2 adsorption isotherms were collected at a range of temperatures from 25 to 100 °C (Figure 4). At temperatures ≤ 75 °C, step-shaped adsorption of CO_2 is apparent, with the step occurring at higher pressures as the temperature increases. Consistent with the isobaric data (Figure 3b), the CO_2 isotherm for dmpn–Mg_2(dobpdc) at 100 °C is nearly flat up to a pressure of 1 bar. Based on the single-component isotherm data of dmpn–Mg_2(dobpdc), adsorption at 150 mbar of CO_2 at 40 °C (2.91 mmol/g, 11 wt%) and desorption under 1 bar of CO_2 at 100 °C (0.49 mmol/g, 1.9 wt %) produces a high working capacity of 2.42 mmol/g (9.1 wt%) with only a 60 °C temperature swing. Using the crystallographic density of activated dmpn–Mg_2(dobpdc) (0.94 g/cm^3), this corresponds to an approximate volumetric working capacity of 2.28 mmol/cm^3 (51 v/v).

Surprisingly, the height and sharpness of the CO_2 adsorption steps were also affected by temperature, with sharper, taller steps observed at lower temperatures and broader, shorter steps observed at higher temperatures. Similar behavior was observed in isobaric adsorption measurements of dmpn–Mg_2(dobpdc) using gas streams with decreasing partial pressures of CO_2 (Figure S10). In contrast, other adsorbents in this family,[16a-c,17a-c] such as closely related mpn–Mg_2(dobpdc), exhibit CO_2 adsorption steps of equivalent height regardless of the temperature in isothermal measurements (Figure S12) or the partial pressure of CO_2 in isobaric measurements (Figure S15). The fundamentally different response of the CO_2 adsorption step heights of dmpn–Mg_2(dobpdc) to changing conditions compared to other diamine-appended variants of Mg_2(dobpdc) suggests that it adsorbs CO_2 by a different mechanism, as will be discussed in detail below.

The CO_2 adsorption isotherms at 40, 50, and 60 °C in Figure 4 were fit empirically using linear interpolation (Figure S7), which allowed the differential enthalpy of adsorption to be determined at each CO_2 loading using the Clausius–Clapeyron relationship (Figure S8). At a CO_2 loading of 1 mmol/g (*i.e.*, in the adsorption step), a differential enthalpy of adsorption (Δh_{ads}) of –74 ± 1 kJ/mol was determined for dmpn–Mg_2(dobpdc), which is comparable to that of other diamine-appended variants of Mg_2(dobpdc)[16a] as well as mpn–Mg_2(dobpdc) (−71 ± 4 kJ/mol, Figure S13) and pn–Mg_2(dobpdc) (−76 ± 2 kJ/mol, Figure S17). Using the low reversible heat capacity (1.5 J/g·°C) of dmpn–Mg_2(dobpdc) (Figure S28), an approximate regeneration energy of 2.1 MJ/kg CO_2 was calculated (see Supporting Information Section 6 for details). This value is approximately half that required to regenerate a 30% monoethanolamine solution (4.8 MJ/kg CO_2),[20] less than that for zeolite 5A (approximately 3.2 MJ/kg CO_2),[21] and similar to that of *N,N′*-dimethylethylenediamine–Mg_2(dobpdc) (2.3 MJ/kg CO_2).[16b] However, all of these adsorbents must be heated to significantly higher temperatures (120,[20] 150,[21] and 140 °C,[16a] respectively) than dmpn–Mg_2(dobpdc) (100 °C) to fully desorb CO_2. Notably, dmpn–Mg_2(dobpdc) also adsorbs only negligible amounts of N_2 (0.017 mmol/g at 750 mbar) and O_2 (0.002 mmol/g at 40 mbar) at 40 °C, leading to excellent CO_2/N_2 (882) and CO_2/O_2 (517) noncompetitive selectivities at the partial pressures relevant for a coal flue gas stream (Figure S11 and Table S1).[11d]

The similar differential enthalpies of CO_2 adsorption in dmpn–, mpn–, and pn–Mg_2(dobpdc) are surprising given the significantly higher step pressure of dmpn–Mg_2(dobpdc), as our previous work suggested that the differential enthalpy should dictate the CO_2 step pressure.[16a,b] We previously observed that the differential enthalpies and entropies of adsorption at a loading of 1 mmol/g (*i.e.,* in the step) are linearly correlated for alkylethylenediamine-functionalized variants of Mg_2(dobpdc) (gray circles, Figure 5, see Table S3 for individual values).[16a] In this plot, isothermal CO_2 step pressures decrease moving towards the upper right corner, as indicated by both stronger CO_2 binding (more negative Δh_{ads}) and reduced CO_2 and diamine mobility (more negative Δs_{ads}) in the adsorbed phase. Both mpn–Mg_2(dobpdc) and pn–Mg_2(dobpdc) obey this relationship and possess 40 °C step pressures (~0.5 mbar) similar to those of adsorbents with comparable differential enthalpies of adsorption.[16a,b]

Performing the same analysis for dmpn–Mg_2(dobpdc), however, revealed it to be an outlier from this trend (black line, Figure 5), as it possesses a more negative differential entropy of adsorption (Δs_{ads} = −204 ± 4 J/mol·K) than expected given its highly exothermic differential enthalpy of adsorption (Δh_{ads} = −74 ± 1 kJ/mol). This increase in the entropic penalty for CO_2 adsorption in dmpn–Mg_2(dobpdc) over what would be predicted from the linear trendline followed by other alkyldiamines (−181 J/mol·K) leads to a Δg_{ads} at 40 °C of –10 ± 2 kJ/mol. Importantly, this value is within error of the Δg_{ads} calculated to be necessary to achieve step-shaped adsorption of CO_2 at 15 mbar and 40 °C (−10.9 kJ/mol), as indicated by its position on the dashed green line in Figure 5. Although dmen–Mg_2(dobpdc)[17a] also lies on this line, it exhibits a less negative Δh_{ads} (−63 ± 4 kJ/mol) than dmpn–Mg_2(dobpdc) (−74 ± 1 kJ/mol), which contributes to the larger temperature swing (ΔT = 76 °C) required to move the adsorption step past 1 bar of CO_2 (eq. 1). The significant change in the differential entropy of adsorption between dmpn–Mg_2(dobpdc) and mpn–Mg_2(dobpdc) and pn–Mg_2(dobpdc) predominantly accounts for the difference in step pressures between these adsorbents at 40 °C (Figure 3a). Notably, this represents a rare instance in which the adsorption properties of a material have been tuned by changing the differential entropy of adsorption.

Performance Under Humid Flue Gas Conditions.

Although dmpn–Mg_2(dobpdc) shows promising properties in single component measurements, assessing its performance for carbon capture under humid conditions is imperative due to the high water content (5–7%) of coal flue gas. In general, materials bearing open metal coordination sites adsorb water and CO_2 at the same binding sites, with more favorable adsorption of water, generally leading water to outcompete CO_2 in multicomponent measurements.[12a,b,22] In contrast, isothermal measurements confirm that the average differential heat of adsorption for water in dmpn–Mg_2(dobpdc) is –47 ± 1 kJ/mol (Figures S29 and S30), which is less negative than that for CO_2 (−73 ± 1 kJ/mol) due to the different binding modes of these two adsorbates. However, these single-component measurements do not necessarily reflect the ability of dmpn–Mg_2(dobpdc) to competitively adsorb CO_2 under humid conditions.

Multicomponent measurements of CO_2 adsorption in the presence of water are more informative for evaluating the potential of dmpn–Mg_2(dobpdc) for carbon capture.[12b] Therefore, we performed humid thermogravimetric analysis (TGA) measurements by bubbling the incident gas stream through water to study the ability of dmpn–Mg_2(dobpdc) to adsorb CO_2 under humid conditions (Figure 6). One drawback of these measurements is that the exact composition of gases adsorbed cannot be reliably determined, although comparison of the mass changes observed with different gas streams provides insight into the behavior of the adsorbent under dry and humid conditions. Consistent with isothermal data (Figure S11), dmpn–Mg_2(dobpdc) adsorbs a negligible amount of dry N_2 at 40 °C (dark blue, Figure 6). Therefore, N_2 co-adsorption can assumed to be negligible in these multicomponent measurements. Cooling dmpn–Mg_2(dobpdc) below 60 °C under a humid N_2 stream led to an increase in mass relative to the dry N_2 isobar. The difference between the dry and humid N_2 cooling isobars should primarily be due to water adsorption and suggests that 1.58 g water per 100 g of adsorbent (0.22 molecules per diamine) are taken up at 40 °C in the absence of CO_2.[23] Importantly, step-shaped adsorption of H_2O was not observed in this assay, suggesting that any step-shaped adsorption observed with humidified CO_2 streams results from CO_2 adsorption.

Cooling dmpn–Mg_2(dobpdc) under a stream of dry 15% CO_2 in N_2 led to step-shaped adsorption of CO_2 (green, Figure 6), with a CO_2 uptake of 14.3 g/100 g (3.24 mmol/g) at 40 °C. This is comparable to the 2.91 mmol/g of CO_2 adsorbed at 150 mbar in the 40 °C isotherm (Figure 3a). Significantly, step-shaped adsorption was also observed upon cooling dmpn–Mg_2(dobpdc) under humid 15% CO_2 in N_2 (light blue), suggesting that CO_2 capture in dmpn–Mg_2(dobpdc) occurs readily in the presence of water. The apparent CO_2 adsorption step of dmpn–Mg_2(dobpdc) shifted to a slightly higher temperature under the humid gas stream, indicating that water promotes CO_2 adsorption. The same increase in apparent CO_2 adsorption step temperature was observed with humidified pure CO_2 and 5% CO_2 in N_2 streams (Figures S32 and S33). This effect is likely due to water stabilizing the CO_2 adsorbed phase through hydrogen-bonding or ion-dipole interactions, as has been observed with other amine-functionalized materials.[15,24] Consistent with this hypothesis, dmpn–Mg_2(dobpdc) exhibits a greater increase in mass after the adsorption step under humid conditions compared to dry conditions. This increased uptake suggests that dmpn–Mg_2(dobpdc) co-adsorbs significantly more water after CO_2 adsorption, leading to an additional uptake of 9.98 g/100 g (5.55 mmol/g if all water, see below) at 40 °C under humid 15% CO_2 in N_2 compared to the dry stream (Figure 6). Together, these findings indicate favorable interactions between water and adsorbed CO_2 in dmpn–Mg_2(dobpdc), which could lead to enhanced uptake of low partial pressures of CO_2 under humid conditions.

To corroborate these promising TGA results, we also performed breakthrough experiments using 0.63 g of semi-spherical dmpn–Mg_2(dobpdc) pellets (350–700 μm diameter) in a stainless steel column with a total packed adsorbent volume of 2.19 cm^3 (Figure 7, see Supporting Information Section 7 for further details). First, breakthrough measurements with a dry 15% CO_2 in N_2 stream were carried out. Near immediate breakthrough of N_2 was observed (blue circles, capacity: < 0.1 mmol/g), followed by sharp breakthrough of CO_2 (green circles, capacity: 2.7 mmol/g) after approximately 30 min at a flow rate of 10 sccm. The incident stream was then switched to He that had been bubbled through water at room

temperature, and the dmpn–Mg_2(dobpdc) was humidified at 40 °C until water breakthrough was detected at the end of the column. Several breakthrough adsorption cycles at 40 °C were then carried out on the water-saturated bed using a stream of 15% CO_2 in N_2 that was humidified by bubbling through CO_2-saturated water at room temperature (~2% water). Similar to the dry breakthrough results, the facile separation of N_2 (purple circles, capacity: < 0.1 mmol/g) and CO_2 could be achieved under humid conditions. Moreover, the CO_2 breakthrough curve became sharper in the presence of water (black circles), leading to a slightly higher CO_2 capacity of 3.0 mmol/g compared to the dry breakthrough measurements. These breakthrough measurements confirm that dmpn–Mg_2(dobpdc) shows superior adsorption of CO_2 under humid conditions compared to dry conditions, making it effective for the removal of CO_2 from a coal flue gas stream.

Another critical factor for employing dmpn–Mg_2(dobpdc) is its long-term stability to adsorption/desorption cycling under humid conditions. This stability was examined by subjecting dmpn–Mg_2(dobpdc) to 1000 simulated adsorption (humid 15% CO_2 in N_2, 5 min, 40 °C) and desorption (humid CO_2, 1 min, 100 °C) cycles, the results of which are summarized in Figure 8. The adsorption and desorption capacities (black circles), as well as the CO_2/H_2O cycling capacity (blue circles), remained constant during the last 200 cycles (see Figure S36 for the raw cycling data). In addition, the adsorbent maintained crystallinity and a high diamine loading of 97% after both 300 and 1000 cycles, confirming that dmpn–Mg_2(dobpdc) is stable to both diamine loss and degradation upon long-term cycling in the presence of water. Some permanently adsorbed species (~7.4 g/100 g, ~4.1 mmol/g if all water) slowly built up during the first 100 cycles, though a high cycling capacity of ~10 g/100 g (~2.3 mmol/g if all CO_2) was still achieved over the last 200 cycles with only a 60 °C temperature swing.[25] Very short adsorption (5 min) and desorption (1 min) intervals could be used in this cycling experiment, reflecting the fast CO_2/H_2O adsorption and desorption kinetics of dmpn–Mg_2(dobpdc). Overall, the dry and humid adsorption measurements indicate that dmpn–Mg_2(dobpdc) is an excellent adsorbent for carbon capture from coal flue gas.

Mechanism of CO_2 Adsorption.

Metal Effect on CO_2 Adsorption Step Pressure.—We initially hypothesized that the CO_2 adsorption step in dmpn–Mg_2(dobpdc) originated from the cooperative formation of ammonium carbamate chains, similar to the behavior previously reported for related frameworks.[16a,b] However, the unusual CO_2 adsorption profile (Figures 3 and 4) and deviation from the linear relationship between Δh_{ads} and Δs_{ads} followed by other adsorbents in this family (Figure 5) suggested a change in the adsorption mechanism for dmpn–Mg_2(dobpdc). One diagnostic feature of ammonium carbamate chain formation is a metal effect on the CO_2 adsorption step pressure, because this mechanism involves breaking a M—N bond and forming a M—O bond.[16b] To probe any potential metal effect on the CO_2 adsorption step, dmpn–M_2(dobpdc) (M = Mn, Co, Ni, Zn) were synthesized and compared to the Mg analogue (see Supporting Information Section 4 for details). The CO_2 adsorption isotherms for dmpn–M_2(dobpdc) (M = Mg, Mn, Co, Zn) at 25 °C confirm that these adsorbents undergo step-shaped adsorption of CO_2 (Figure 9). The distinctive isotherm shapes of dmpn–M_2(dobpdc) (M = Mn, Co, Zn) are similar to that of the Mg analogue,

suggesting that these materials adsorb CO_2 via a similar uptake mechanism. Consistent with cleavage of the M—N bond during CO_2 adsorption, the CO_2 adsorption step pressures increase in the order Mg < Mn < Co ≈ Zn, which is the same order previously observed for M_2(dobpdc) variants appended with *N,N′*-dimethylethylenediamine[16b] and trends with increasing M—N bond strength.[26] In addition, the diagnostic C–N stretch of an ammonium carbamate at ~1330 cm^{-1} was observed in the IR spectra of CO_2-dosed samples of dmpn–M_2(dobpdc) (M = Mg, Mn, Co, Zn) (Figures S41 and 42).[15a,16a,b] Taken together, these findings support the formation of ammonium carbamate chains in dmpn–M_2(dobpdc) (M = Mg, Mn, Co, Zn). Notably, as with alkylethylenediamine-appended variants,[16b] dmpn–Ni_2(dobpdc) did not display step-shaped adsorption of CO_2 and thus likely adsorbs CO_2 via a distinct mechanism.

Solid-State ^{13}C NMR Experiments.—To further probe the CO_2 adsorption mechanism in dmpn–Mg_2(dobpdc), magic angle spinning (MAS) solid-state ^{13}C NMR measurements with isotopically enriched $^{13}CO_2$ were carried out (Figures 10 and 11). Using $^{13}CO_2$ improved the signal-to-noise ratio of these spectra and allowed for short acquisition times (~30 min).[27] In addition, a custom dosing manifold enabled the preparation of samples dosed with different pressures of $^{13}CO_2$ and thus for the examination of the uptake mechanism at different points in the CO_2 adsorption isotherms (see Supporting Information Section 8 for details).

To serve as a point of reference, the ^{13}C NMR spectrum of $^{13}CO_2$-dosed dmen–Mg_2(dobpdc)[17a] (Figure 10) was collected, as the single-crystal X-ray diffraction structure of dmen–Zn_2(dobpdc) confirms that it forms ammonium carbamate chains (Figure S47). Consistent with the literature,[17a] the ^{13}C NMR spectrum of dmen–Mg_2(dobpdc) displays a new resonance at 163.7 ppm upon exposure to $^{13}CO_2$ (Figure 10a). This same resonance was observed at both moderate (129 mbar) and high (989 mbar) pressures of $^{13}CO_2$. Previous solid-state NMR studies of amine-appended silicas assign resonances with this chemical shift to the carbonyl carbon of an ammonium carbamate species.[28] The remainder of the spectrum features assignable resonances from the framework and diamine comparable to the spectrum obtained before $^{13}CO_2$ dosing (Figure S39), supporting the formation of one dominant ammonium carbamate species upon exposure to $^{13}CO_2$.

The ^{13}C NMR spectra of pn–Mg_2(dobpdc)–$^{13}CO_2$ and mpn–Mg_2(dobpdc)–$^{13}CO_2$ are similar to that of dmen–Mg_2(dobpdc)–$^{13}CO_2$, with a single dominant resonance observed at 162.7 and 162.8 ppm, respectively (Figure 10b,c). In both cases, the same dominant chemisorbed species was observed at low and high pressures of $^{13}CO_2$, although a slight shoulder was observed at ~159 ppm in the spectrum of pn–Mg_2(dobpdc) at 980 mbar of $^{13}CO_2$. In addition, the IR spectra of CO_2-dosed samples of mpn– and pn–Mg_2(dobpdc) display new stretches at ~1330 cm^{-1} corresponding to the C–N stretch of an ammonium carbamate species (Figure S41).[15a,16a,b] Taken together, these findings suggest that mpn– and pn–Mg_2(dobpdc) predominantly form ammonium carbamate chains upon CO_2 adsorption. Unfortunately, we have thus far been unable to structurally characterize the CO_2-adsorbed phases of mpn– or pn–M_2(dobpdc) variants to confirm this hypothesis.

In contrast, the ^{13}C NMR spectrum of dmpn–Mg_2(dobpdc)–$^{13}CO_2$ is significantly more complex, with at least two resonances corresponding to the carbonyl carbon atoms of chemisorbed species observed at 164.2 and 161.1 ppm under 29 mbar of $^{13}CO_2$ (Figure 11a). At higher pressures (88 and 1072 mbar), three resonances result from chemisorbed $^{13}CO_2$. Additional splitting of the amine resonances is also apparent, particularly at 1072 mbar, supporting the formation of multiple chemisorbed species. By comparison with the ^{13}C NMR spectra shown in Figure 10, as well as with the literature,[28] we assign the downfield resonance at 164.2 ppm that dominates immediately after the CO_2 adsorption step (29 mbar) as arising from ammonium carbamate chains. Due to the low step pressure of dmpn–Mg_2(dobpdc) at room temperature (~5 mbar), we have thus far been unable to obtain ^{13}C NMR spectra at $^{13}CO_2$ pressures below the adsorption step.

The higher step pressure of dmpn–Zn_2(dobpdc) (~100 mbar, 25 °C) compared to dmpn–Mg_2(dobpdc) (~5 mbar, 25 °C) allowed for the acquisition of ^{13}C NMR spectra before and after the adsorption step (Figure 11b). At partial pressures of $^{13}CO_2$ below the adsorption step (79 and 87 mbar), a number of weak broad resonances arise from chemisorbed $^{13}CO_2$ (160–165 ppm). These relatively weak signals result from the minor amounts of $^{13}CO_2$ (≤0.5 mmol/g) adsorbed at these pressures (Figure 9). Increasing the $^{13}CO_2$ pressure past the CO_2 adsorption step (156 and 304 mbar) results in two sharp resonances at 164.4 and 160.1 ppm and splitting of the resonances corresponding to the framework and diamine into several peaks. By comparison with the literature[28] and the other ^{13}C NMR spectra presented in Figure 10, we assign the downfield resonance at 164.4 ppm in these spectra to ammonium carbamate chains. Indeed, density functional theory (DFT) calculations using a putative ammonium carbamate chain structure for dmpn–Zn_2(dobpdc)-CO_2 yielded a predicted chemical shift of 165.3 ppm (Figure S40). Thus, the NMR experiments indicate that the ammonium carbamate species observed by both ^{13}C NMR and IR spectroscopy is partly responsible for the adsorption step at ~100 mbar at 25 °C.

Interestingly, at higher pressures of $^{13}CO_2$ (842 and 1038 mbar) the two resonances observed at intermediate pressures greatly decrease in intensity, leading a hitherto unidentified species (161.1 ppm) to dominate at 1038 mbar. In contrast, for dmpn–Mg_2(dobpdc) the assigned ammonium carbamate chains (164.2 ppm) are apparent even at high pressures of $^{13}CO_2$ (1072 mbar), reflecting their more stable nature compared to those of the Zn analogue.[16b] Although it is perhaps unsurprising that dmpn–M_2(dobpdc) (M = Mg, Mn, Co, Zn) analogues form ammonium carbamate species upon CO_2 adsorption in view of the reactivity of related diamine-appended metal–organic frameworks,[16a,b] the identity of the other chemisorbed species in the ^{13}C NMR spectra of dmpn–M_2(dobpdc) (M = Mg, Zn) was not immediately apparent.

3.3.3 Single-Crystal X-ray Diffraction Studies.—We turned to single-crystal X-ray diffraction in order to identify the species observed at 161.1 ppm that dominates the ^{13}C NMR spectrum of dmpn–Zn_2(dobpdc) at higher pressures of $^{13}CO_2$ (Figure 11). The structure of diethyl ether-solvated dmpn–Zn_2(dobpdc) was first obtained in the absence of CO_2 (Figure 12a). Importantly, considerable unobstructed pore volume remains after diamine grafting (Figure S45), consistent with the high Brunauer-Emmett-Teller (BET) surface area of 948 ± 3 m^2/g determined for dmpn–Mg_2(dobpdc) from the N_2 adsorption

isotherm at 77 K (Figure S6). This should allow for rapid diffusion of CO_2 into and out of the pores. Interestingly, the presence of an extensive hydrogen bonding network between adjacent diamines can be inferred from the close N···N contacts of 3.26(3) Å. In addition, the powder X-ray diffraction pattern of dmpn–Mn_2(dobpdc) is consistent with the presence of a similar hydrogen bonding network (see Section 10 of the Supporting Information). Likewise, the single-crystal structure of toluene-solvated mpn–Zn_2(dobpdc) shows two distinct conformations involving hydrogen-bonding between amines; the minor conformer involves hydrogen-bonding along the *c*-axis, as in Figure 12a (30.8(13)% occupancy), whereas the major conformer (57.1(13)% occupancy) involves intramolecular hydrogen bonding between the terminal and metal-bound amines of a single diamine (Figure S46). These interactions are not available to alkylethylenediamine-appended variants of Zn_2(dobpdc) because adjacent diamines are unable to reach one another down the *c*-axis[16a,b] and likely contribute significantly to the observed stability of dmpn–Mg_2(dobpdc) to adsorption/desorption cycling (Figure 8).

Remarkably, dosing activated single crystals of dmpn–Zn_2(dobpdc) with 1 bar of CO_2 allowed us to obtain the X-ray diffraction structure corresponding to the unidentified species observed by solid-state ^{13}C NMR spectroscopy (Figure 11). In contrast to all other diamine-appended metal organic frameworks studied to date,[16a,b] dmpn–Zn_2(dobpdc) was found to form carbamic acid pairs bridging diagonally adjacent diamines upon exposure to CO_2 (Figure 12b, Figure 13). While the bridging hydrogen atoms could not be located in the structure, their presence was inferred from the close O···O contacts of 2.38(4) and 2.88(4) Å, respectively. These pairs are connected by hydrogen-bonding interactions along the *c*-axis and thus form an extended ladder-like structure running down the pores of the framework (Figure 12b). Importantly, significant unoccupied pore volume remains even after CO_2 adsorption, enabling facile gas transport through the pores (Figure 13). Although previous DFT calculations suggested that the formation of carbamic acid pairs would not be expected to proceed cooperatively,[29] the presence of hydrogen-bonding interactions along the *c*-axis in this structure may impart some degree of cooperativity. However, such interactions are also present in the absence of CO_2 (Figure 12a), and therefore any cooperative effects are likely offset by similar hydrogen-bonding interactions between adjacent carbamic acid pairs, between carbamic acid pairs and adjacent free amines, and between adjacent free amines. Therefore, the carbamic acid pairs likely dominate in the post-step regimes of the CO_2 isotherms of dmpn–M_2(dobpdc) (M = Mg, Mn, Co, Zn), with insertion to form ammonium carbamate chains occurring predominantly near the CO_2 adsorption step. The combination of a primarily non-cooperative adsorption isotherm for the carbamic acid pairs and a step-shaped adsorption isotherm for the ammonium carbamate chains likely gives rise to the distinct isotherm shapes of dmpn-functionalized analogues of M_2(dobpdc). Notably, dmpn–Ni_2(dobpdc), which possesses M—N bonds that are too strong to allow for CO_2 insertion to form ammonium carbamate chains,[16b] likely adsorbs CO_2 exclusively via the formation of carbamic acid pairs and exhibits a non-cooperative adsorption profile.

Although carbamic acid pairs have not been experimentally observed in a diamine-appended metal–organic framework until now, previous DFT calculations found that carbamic acid pairs of a different geometry were comparable in energy to the experimentally observed ammonium carbamate chains with *N,N′*-dimethylethylenediamine in place of dmpn.[16b,29]

The formation of hydrogen-bond stabilized carbamic acids upon reaction with CO_2 has also been proposed in certain amine-functionalized adsorbents,[15a,b,30] but this adsorption mechanism has recently been called into doubt[31] due to the known instability of carbamic acids.[32] Therefore, to the best of our knowledge, the present results constitute the first crystallographic observation of carbamic acid pair formation in a porous solid[33,34] and thus serve as corroborating evidence for the formation of carbamic acid species stabilized by hydrogen-bonding in other adsorbents. Consistent with this assessment, the solid-state ^{13}C NMR resonances previously ascribed to carbamic acid species were observed at ~160 ppm,[28] similar in chemical shift to the resonance at 161.1 ppm we assign to carbamic acid pairs in the ^{13}C NMR spectra of dmpn–Zn_2(dobpdc) (Figure 11). In addition, DFT calculations using the single-crystal X-ray diffraction structure (Figure 12b) afforded a predicted chemical shift of 161.1 ppm for the observed carbamic acid pairs (see Supporting Information Section 8 for details). Based on this assignment, the species observed at intermediate pressures (156 and 304 mbar) at 160.1 ppm in the ^{13}C NMR spectra of dmpn–Zn_2(dobpdc) is possibly an unpaired carbamic acid intermediate. Together, the ^{13}C NMR and X-ray diffraction experiments corroborate that dmpn–M_2(dobpdc) (M = Mg, Mn, Co, Zn) form a complex mixture of ammonium carbamate and carbamic acid species upon CO_2 adsorption.

CONCLUSION

Through careful consideration of the thermodynamics of CO_2 adsorption in diamine-appended metal–organic frameworks, we have developed a new adsorbent, dmpn–Mg_2(dobpdc), that is well-tuned for the efficient capture of CO_2 from coal flue gas. Specifically, the highly negative differential enthalpy of adsorption (Δh_{ads} = −74 ± 1 kJ/mol) facilitates the effective capture of CO_2 at 40 °C and near complete regeneration at 100 °C under 1 bar of CO_2, whereas the larger than expected entropic penalty for CO_2 adsorption (Δs_{ads} = −204 ± 4 J/mol·K) moves the step to a higher pressure at a given temperature. With this new adsorbent, a narrow temperature swing (ΔT = 60 °C) can be used to achieve a high CO_2 working capacity of 2.42 mmol/g (9.1 wt%) in a TSA process, which should help to dramatically lower the energy penalty associated with carbon capture and sequestration. Importantly, dmpn–Mg_2(dobpdc) also exhibits exceptional long-term stability and maintains its performance under humid conditions. Efforts are now underway to evaluate the use of dmpn–Mg_2(dobpdc) for large-scale CO_2 capture applications.

The NMR studies presented herein suggest that the mechanistic possibilities for the uptake of CO_2 in diaminopropane-appended metal–organic frameworks are more complex than with ethylenediamines, as the latter appear to adsorb CO_2 solely via cooperative formation of ammonium carbamate chains (Figure 10a).[16a,b] In particular, the addition of a single methyl group to the diamine backbone (from mpn to dmpn) drastically changes the CO_2 adsorption step pressure (Figure 3a), differential entropy of adsorption (Figure 5), and CO_2 adsorption mechanism (Figures 10-12). Relatedly, single-crystal X-ray diffraction and ^{13}C NMR experiments demonstrate for the first time that carbamic acid pair formation is feasible and can occur competitively with ammonium carbamate chain formation in a diamine-appended metal–organic framework. Additional structural and NMR investigations are underway to fully understand the effect of diaminopropane structure, metal, CO_2 partial

pressure, temperature, and humidity on the mechanisms of CO_2 adsorption in dmpn–Mg_2(dobpdc). One critical area for further experimental and theoretical investigation is the relationship between bridging carbamic acid pairs and ammonium carbamate chains, particularly regarding the cooperative adsorption of CO_2. Given the exceptional promise of dmpn–Mg_2(dobpdc) for the efficient capture from coal flue gas, these studies should prove valuable for developing next generation adsorbents for carbon capture applications.

Supplementary Material

Refer to Web version on PubMed Central for supplementary material.

ACKNOWLEDGMENT

We acknowledge ExxonMobil Research and Engineering Company for funding the initial synthesis and characterization of pn–, mpn–, and dmpn–Mg_2(dobpdc) as part of a carbon capture research project. Crystallographic and solid-state NMR studies were supported through the Center for Gas Separations Relevant to Clean Energy Technologies, an Energy Frontier Research Center funded by the U.S. Department of Energy (DoE), Office of Science, Office of Basic Energy Sciences, under Award DE-SC0001015. The collection and analysis of adsorption data for dmpn–Mg_2(dobpdc) for CCS applications was supported by the U.S./China Clean Energy Research Center for Water-Energy Technologies (CERC-WET). We thank the National Institute of General Medical Sciences of the National Institutes of Health for a postdoctoral fellowship for P.J.M. (F32GM120799). The content is solely the responsibility of the authors and does not necessarily represent the official views of the National Institutes of Health. We thank the Philomathia Foundation and Berkeley Energy and Climate Institute for a fellowship for A.C.F. We thank the Miller Institute for Basic Research in Science for a post-doctoral fellowship for J.D.M. This work utilized the resources of both the Advanced Light Source at Lawrence Berkeley National Laboratory, a user facility supported by the Director, Office of Science, Office of Basic Energy Sciences, of the DoE under Contract No. DE-AC02-05CH11231, and the Advanced Photon Source, DoE Office of Science User Facility operated for the DoE Office of Science by Argonne National Laboratory under Contract No. DE-AC02-06CH11357. Collection of adsorption data for dmen–Mg_2(dobpdc), men–Mg_2(dobpdc), and en–Mg_2(dobpdc) (Supporting Information Section 3) was funded by the Advanced Research Projects Agency – Energy (ARPA-E) of the DoE. Dr. Jarad Mason and Dr. Thomas McDonald are acknowledged for assistance in collecting the CO_2 isotherms of dmen–Mg_2(dobpdc). DFT calculations of ^{13}C NMR chemical shifts were supported by the National Institutes of Health (S10OD023523) via the Molecular Graphics and Computation Facility (College of Chemistry, UC Berkeley). Douglas Reed, Henry Jiang, Julia Oktawiec, Michael Ziebel, Dr. Jun Xu, and Thomas Osborn Popp (UC Berkeley), as well as Dr. Simon C. Weston (ExxonMobil), are acknowledged for experimental assistance and/or helpful discussions. A.C.F. thanks Dr. Richard Bounds for assistance with the design and manufacture of the custom vacuum manifold used for dosing NMR samples with $^{13}CO_2$.

REFERENCES

(1). Pachauri RK; Meyer LA Climate Change 2014: Synthesis Report. Contribution of Working Groups I, II and III to the Fifth Assessment Report of the Intergovernmental Panel on Climate Change; IPCC: Geneva, Switzerland, 2014; p. 1–151.

(2). Quadrelli R; Peterson S Energy Policy 2007, 35, 5938.

(3). Akpan UF; Akpan GE International Journal of Energy Economics and Policy 2012, 2, 21.

(4). Granite EJ; Pennline HW Ind. Eng. Chem. Res 2002, 41, 5470.

(5). (a)Senftle TP; Carter EA Acc. Chem. Res 2017, 50, 472; [PubMed: 28945424] (b)Chu S Science 2009, 325, 1599; [PubMed: 19779157] (c)Haszeldine RS Science 2009, 325, 1647. [PubMed: 19779187]

(6). (a)Bhown AS; Freeman BC Environ. Sci. Technol 2011, 45, 8624; [PubMed: 21905745] (b)House KZ; Harvey CF; Aziz MJ; Schrag DP Energy Environ. Sci 2009, 2, 193.

(7). Drage TC; Snape CE; Stevens LA; Wood J; Wang J; Cooper AI; Dawson R; Guo X; Satterley C; Irons R J. Mater. Chem 2012, 22, 2815.

(8). (a)Boot-Handford ME; Abanades JC; Anthony EJ; Blunt MJ; Brandani S; MacDowell N; Fernández JR; Ferrari M-C; Gross R; Hallet JP; Haszeldine RS; Heptonstall P; Lyngfelt A; Makuch Z; Mangano E; Porter RTJ; Pourkashanian M; Rochelle GT; Shah N; Yao JG; Fennell

PS Energy Environ. Sci 2014, 7, 130;(b)Rochelle GT Science 2009, 325, 1652. [PubMed: 19779188]

(9). (a)Fredriksen SB; Jens K-J Energy Procedia 2013, 37, 1770;(b)Gouedard C; Picq D; Launay F; Carrette P-L Int. J. Greenhouse Gas Control 2012, 10, 244.

(10). Finkeenrath M Cost and Performance of Carbon Dioxide Capture from Power Generation, International Energy Agency, 2011.

(11). (a)(a)For selected reviews, see: For selected reviews, see: Yu J; Xie L-H; Li J-R; Ma Y; Seminario JM; Balbuena PB Chem. Rev 2017, 117, 9674; [PubMed: 28394578] (b)Lee S-Y; Park S-J J. Ind. Eng. Chem. Res 2015, 23, 1;(c)Sabouni R; Kazemian H; Rohani S Environ. Sci. Pollut. Res 2014, 21, 5427;(d)Sumida K; Rogow DL; Mason JA; McDonald TM; Bloch ED; Herm ZR; Bae T-H; Long JR Chem. Rev 2012, 112, 724; [PubMed: 22204561] (e)Liu Y; Wang ZU; Zhou H-C Greenhouse Gasses Sci. Technol 2012, 2, 239;(f)Samanta A; Zhao A; Shimizu GKH; Sarkar P; Gupta R Ind. Eng. Chem. Res 2012, 51, 1438;(g)D'Alessandro DM; Smit B; Long JR Angew. Chem. Int. Ed, 2010, 49, 6058.

(12). (a)For selected examples, see: Woerner WR; Plonka AM; Chen X; Banerjee D; Thallapally PK; Parise JB J. Phys. Chem. C 2016, 120, 360;(b)Mason JA; McDonald TM; Bae T-H; Bachman JE; Sumida K; Dutton JJ; Kaye SS; Long JR J. Am. Chem. Soc 2015, 137, 4787; [PubMed: 25844924] (c)Burtch NC; Jasuja H; Walton KS Chem. Rev 2014, 114, 10575; [PubMed: 25264821] (d)Liu J; Thallapally PK; McGrail BP; Brown DR; Liu J Chem. Soc. Rev 2012, 41, 2308; [PubMed: 22143077] (e)Wang Y; LeVan MD J. Chem. Eng. Data 2010, 55, 3189.

(13). (a)Adsorbents lacking open metal sites tend to be more stable under humid conditions, although their CO_2 capacities under flue gas conditions are modest and their ability to capture CO_2 effectively under humid conditions remains uncertain (see ref. 12b for further details). For selected examples, see: Nandi S; Collins SP; Chakraborty D; Banerjee D; Thallapally PK; Woo TK; Vaidhyanathan R J. Am. Chem. Soc 2017, 139, 1734; [PubMed: 28107782] $_{22}$(b)Bhatt PM; Belmabkhout Y; Cadiau A; Adil K; Shekhah O; Shkurenko A; Barbour LJ; Eddaoudi M J. Am. Chem. Soc 2016, 138, 9301; [PubMed: 27388208] (c)Elsaidi SK; Mohamed MH; Schaef HT; Kumar A; Lusi M; Pham T; Forrest KA; Space B; Xu W; Halder GJ; Liu J; Zaworotko MJ; Thallapally PK Chem. Commun 2015, 51, 15530;(d)Nugent P; Belmabkhout Y; Burd SD; Cairns AJ; Luebke R; Forrest K; Pham T; Ma S; Space B; Wojtas L; Eddaoudi M; Zaworotko MJ Nature 2013, 495, 80. [PubMed: 23446349]

(14). (a)Ünveren EE; Monkul BO; Sarioğlan S; Karademir N; Alper E Petroleum 2017, 3, 37;(b)Kim C; Cho HS; Chang S; Cho SJ; Choi M Energy Environ. Sci 2016, 9, 1803;(c)Lin Y; Kong C; Chen L RSC Adv. 2016, 6, 32598;(d)Bollini P; Didas SA; Jones CW J. Mater. Chem 2011, 21, 15100.

(15). (a)For selected examples, see: Didas SA; Sakwa-Novak MA; Foo GS; Sievers C; Jones CW J. Phys. Chem. Lett 2014, 5, 4194; [PubMed: 26278953] (b)Bacsik Z; Ahlsten N; Ziadi A; Zhao G; Garcia,bennett AE; Martín-Matute B; Hedin N Langmuir 2011, 27, 11118; [PubMed: 21774480] (c)Sayari A; Belmabkhout Y J. Am. Chem. Soc 2010, 132, 6312; [PubMed: 20405941] (d)Serna-Guerrero R; Da'na E; Sayari A Ind. Eng. Chem. Res 2008, 47, 9406.

(16). (a)Siegelman RL; McDonald TM; Gonzalez MI; Martell JD; Milner PJ; Mason JA; Berger AH; Bhown AS; Long JR J. Am. Chem. Soc. 2017, 139, 10526; [PubMed: 28669181] (b)McDonald TM; Mason JA; Kong X; Bloch ED; Gygi D; Dani A; Crocellà V; Giordanino F; Odoh SO; Drisdell WS; Vlaisavljevich B; Dzubak AL; Poloni R; Schnell SK; Planas N; Lee K; Pascal T; Wan LF; Prendergast D; Neaton JB; Smit B; Kortright JB; Gagliardi L; Bordiga S; Reimer JA; Long JR Nature 2015, 519, 303; [PubMed: 25762144] (c)McDonald TM; Lee WR; Mason JA; Wiers BM; Hong CS; Long JR J. Am. Chem. Soc. 2012, 134, 7056. [PubMed: 22475173] (d)See also: Drisdell WS; Poloni R; McDonald TM; Pascal TA; Wan LF; Pemmaraju CD; Vlaisavlievich B; Odoh SO; Neaton JB; Long JR; Prendergast D; Kortright JB Phys Chem Chem Phys 2015, 17, 2144;(e)McDonald TM; D'Alessandro DM; Krishna R; Long JR Chem. Sci. 2011, 2, 2022; (f)Demessence A; D'Alessandro DM; Foo ML; Long JR J. Am. Chem. Soc. 2009, 131, 8784. [PubMed: 19505094]

(17). (a)For the functionalization of Mg_2(dobpdc), see: Jo H; Lee WR; Kim NW; Jung H; Lim KS; Kim JE; Kang DW; Lee H; Hiremath V; Seo JG; Jin H; Moon D; Han SS; Hong CS ChemSusChem 2017, 10, 541; [PubMed: 28004886] $_2$(b)Lee WR; Jo H; Yang L-M; Lee H; Ryu DW; Lim KS; Song JH; Min DY; Han SS; Seo JG; Park YK; Moon D; Hong CS Chem. Sci 2015,

6, 3697; [PubMed: 28706716] (c)Lee WR; Hwang SY; Ryu DW; Lim KS; Han SS; Moon D; Choi J; Hong CS Energy Environ. Sci 2014, 7, 744.For the functionalization of other open-metal site metal–organic frameworks with diamines, see: (d) Liao P-Q; Chen X-W; Liu S-Y; Li X-Y; Xu Y-T; Tang M; Rui Z; Ji H; Zhang J-P; Chen X-M Chem. Sci 2016, 7, 6528; [PubMed: 27928493] (e)Darunte LA; Oetomo AD; Walton KS; Sholl DS; Jones CW ACS Sustainable Chem. Eng 2016, 4, 5761;(f)Yeon JS; Lee WR; Kim NW; Jo H; Lee H; Song JH; Lim KS; Kang DW; Seo JG; Moon D; Wiers B; Hong CS J. Mater. Chem. A 2015, 3, 19177;(g)Cao Y; Song F; Zhao Y; Zhong QJ Environ. Sci 2013, 25, 2081;(h)Hu Y; Verdegaal WM; Yu S-H; Jiang H-L ChemSusChem 2014, 7, 734; [PubMed: 24464970] (i)Lin Y; Lin H; Wang H; Suo Y; Li B; Kong C; Chen LJ Mater. Chem. A 2014, 2, 14658;(j)Choi S; Watanabe T; Bae T-H; Sholl DS; Jones CW J. Phys. Chem. Lett 2012, 3, 1136; [PubMed: 26288048] (k)Montoro C; García E; Calero S; Pérez-Fernández MA; López AL; Barea E; Navarro JAR J. Mater. Chem 2012, 22, 10155.

(18). Campbell CT; Sellers JRV Chem. Rev 2013, 113, 4106. [PubMed: 23441680]

(19). Hefti M; Joss L; Bjelobrk Z; Mazzotti M Faraday Discuss., 2016, 192, 153. [PubMed: 27509258]

(20). Song H-J; Lee S; Park K; Lee J; Spah DC; Park J-W; Filburn TP Ind. Eng. Chem. Res 2008, 47, 9925.

(21). Merel J; Clausse M; Meunier F Ind. Eng. Chem. Res 2008, 47, 209.This value was calculated from the approximate specific heat consumption resulting only from the adsorbent (adsorbent, desorption heat, heat losses) reported in this reference, and not from the entire process (4.41 MJ/kg CO_2).

(22). (a)Datta SJ; Khumnoon C; Lee ZH; Moon WK; Docao S; Nguyen TH; Hwang IC; Moon D; Oleynikov P; Terasaki O; Yoon KB Science 2015, 350, 302; [PubMed: 26472904] (b)Joos L; Swisher JA; Smit B Langmuir 2013, 29, 15936; [PubMed: 24313865] (c)Liu J; Wang Y; Benin AI; Jakubczak P; Willis RR; LeVan MD Langmuir 2010, 26, 14301 [PubMed: 20707342]

(23). Comparing this uptake to the 40 °C water isotherm (Figure S29) suggests the partial pressure of water in the humidified stream is approximately 13 mbar, or 1.3%.

(24). One consequence of this effect is that slightly higher regeneration temperatures were found to be required under humid conditions, although regeneration at 100 °C was still sufficient to desorb CO_2 and water from dmpn–Mg_2(dobpdc) under an atmosphere of humid pure CO_2 (Figure S34).

(25). The permanently adsorbed species (likely both CO_2 and water) could be more completely regenerated from the adsorbent by cycling with a higher regeneration temperature of 110 °C, leading to a higher cycling capacity after 100 cycles (15.2 g/100 g) with no deleterious effect on the stability of the adsorbent (Figure S38). In fact, dmpn–Mg_2(dobpdc) could be cycled with regeneration at temperatures as high as 150 °C, or held under flowing humid CO_2 for 12 h at temperatures as high as 200 °C, with minimal diamine loss. See Supporting Information Section 7 for further details.

(26). Irving H; Williams RJP J. Chem. Soc 1953, 637, 3192.

(27). Because of the low natural abundance of ^{13}C in CO_2, long acquisition times (6 h) were required to obtain ^{13}C NMR spectra with non-isotopically enriched CO_2. This led to pressure changes over the course of the acquisition due to gas leakage from the rotor.

(28). (a)Mafra L; Čendak T; Schneider S; Wiper PV; Pires J; Gomes JRB; Pinto ML J. Am. Chem. Soc 2017, 139, 389; [PubMed: 27951638] (b)Pinto ML; Mafra L; Guil JM; Pires J; Rocha J Chem. Mater 2011, 23, 1387;(c)Moore JK; Sakwa-Novak MA; Chaikittisilp W; Mehta AK; Conradi MS; Jones CW; Hayes SE Environ. Sci. Technol 2015, 49, 13684; [PubMed: 26477882] (d)Foo GS; Lee JJ; Chen C-H; Hayes SE; Sievers C; Jones CW ChemSusChem 2017, 10, 266. [PubMed: 27573047]

(29). (a)Vlaisavljevich B; Odoh SO; Schnell SK; Dzubak AL; Lee K; Planas N; Neaton JB; Gagliardi L; Smit B Chem. Sci 2015, 6, 5177; [PubMed: 28717499] (b)Planas N; Dzubak AL; Poloni R; Lin L-C; McManus A; McDonald TM; Neaton JB; Long JR; Smit B; Gagliardi L J. Am. Chem. Soc 2013, 135, 7402. [PubMed: 23627764]

(30). (a)Fracaroli AM; Furukawa H; Suzuki M; Dodd M; Okajima S; Gándara F; Reimer JA; Yaghi OM J. Am. Chem. Soc 2014, 136, 8863; [PubMed: 24911868] (b)Aziz B; Hedin N; Bacsik Z Microporous Mesoporous Mater. 2012, 159, 42;(c)Bacsik Z; Alturi R; Garcia,bennett AE; Hedin N Langmuir 2010, 26, 10013; [PubMed: 20218553] (d)Knöfel C; Martin C; Hornebecq V;

Llewellyn PL J. Phys. Chem. C 2009, 113, 2172;(e)Dibenedetto A; Pastore C; Fragale C; Aresta M ChemSusChem 2008, 1, 742. [PubMed: 18688908]

(31). Danon A; Stair PC; Weitz E J. Phys. Chem. C 2011, 115, 11540.

(32). (a)Bossa J-B; Borget F; Duvernay F; Theulé P; Chiavassa T J.Phys. Chem. A 2008, 112, 5113; [PubMed: 18491873] (b)Masuda K; Ito Y; Fujita H Tetrahedron 2005, 61, 213;(c)Khanna RK; Moore MH Spectrochim. Acta, Part A 1999, 55, 961.

(33). The formation of carbamic acid pairs upon exposure of dibenzylamine to CO_2 has been confirmed by single-crystal X-ray diffraction. See: Aresta M; Ballivet-Tkatchenko D; Dell'Amico DB; Bonnet MC; Boschi D; Calderazzo F; Faure R; Labella L; Marchetti F Chem. Commun 2000, 1099.$_2$

(34). The single-crystal X-ray diffraction structure of an amine-stabilized carbamic acid was disclosed during the preparation of this manuscript (Inagaki F; Matsumoto C; Itwata T; Mukai CJ Am. Chem. Soc 2017, 139, 4639).However, the NMR and structural evidence could also be consistent with complete proton transfer to form an ammonium carbamate species.

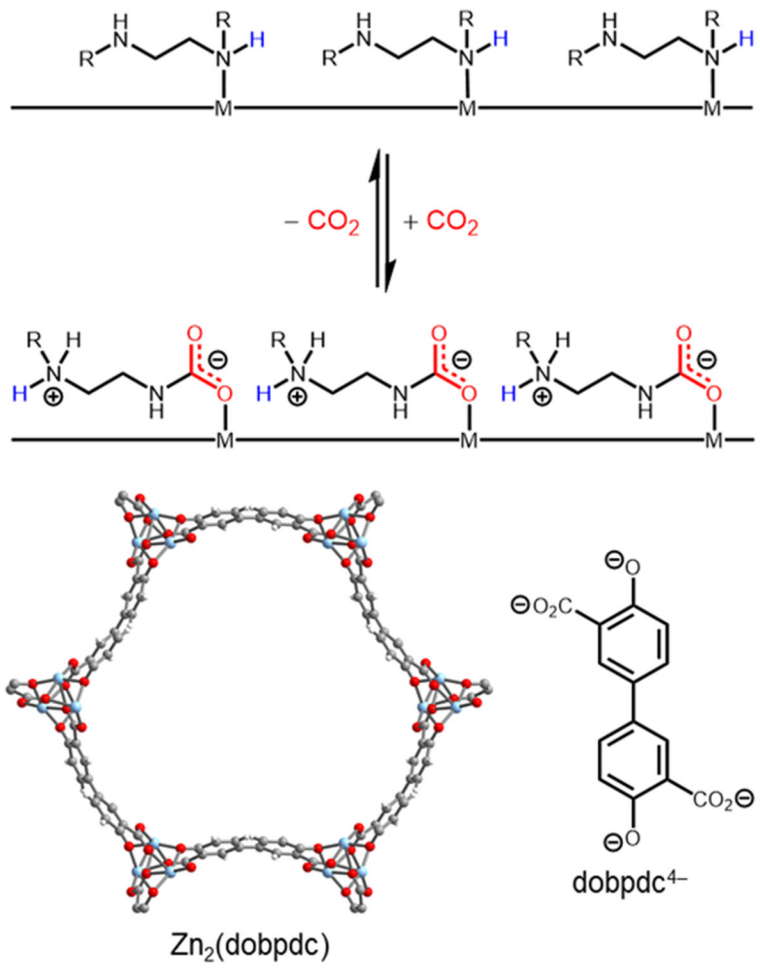

Figure 1.

General structure of alkylethylenediamine-appended variants of M_2(dobpdc) (dobpdc^{4-} = 4,4′-dioxidobiphenyl-3,3′-dicarboxylate), represented by the single-crystal X-ray diffraction structure of the Zn framework, which cooperatively adsorb CO_2 via the formation of ammonium carbamate chains.

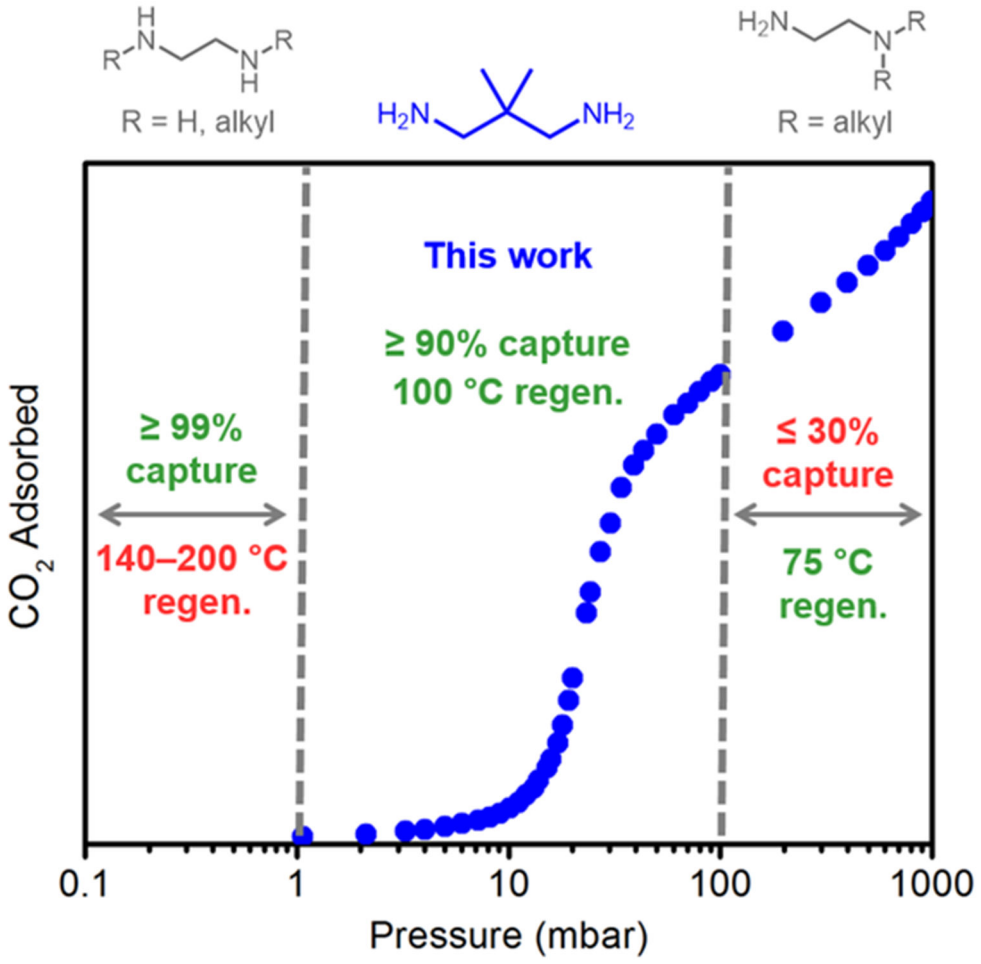

Figure 2.

Summary of 40 °C CO_2 step pressures and regeneration temperatures under 1 bar of CO_2 for alkyldiamine-appended variants of Mg_2(dobpdc).

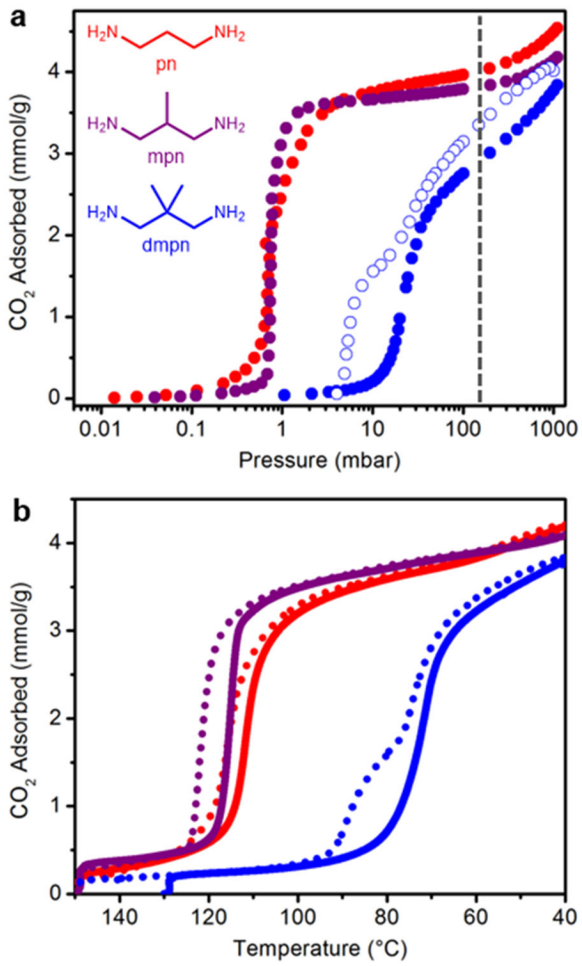

Figure 3.

(a) Isotherms for the adsorption of CO_2 at 40 °C CO_2 in pn–, mpn–, and dmpn–Mg_2(dobpdc) (desorption data shown with open circles). The dashed line indicates the approximate partial pressure of CO_2 in coal flue gas (150 mbar). (b) Adsorption (solid) and desorption (dotted) isobars of pn–, mpn–, and dmpn–Mg_2(dobpdc) under pure CO_2, as measured by thermogravimetric analysis.

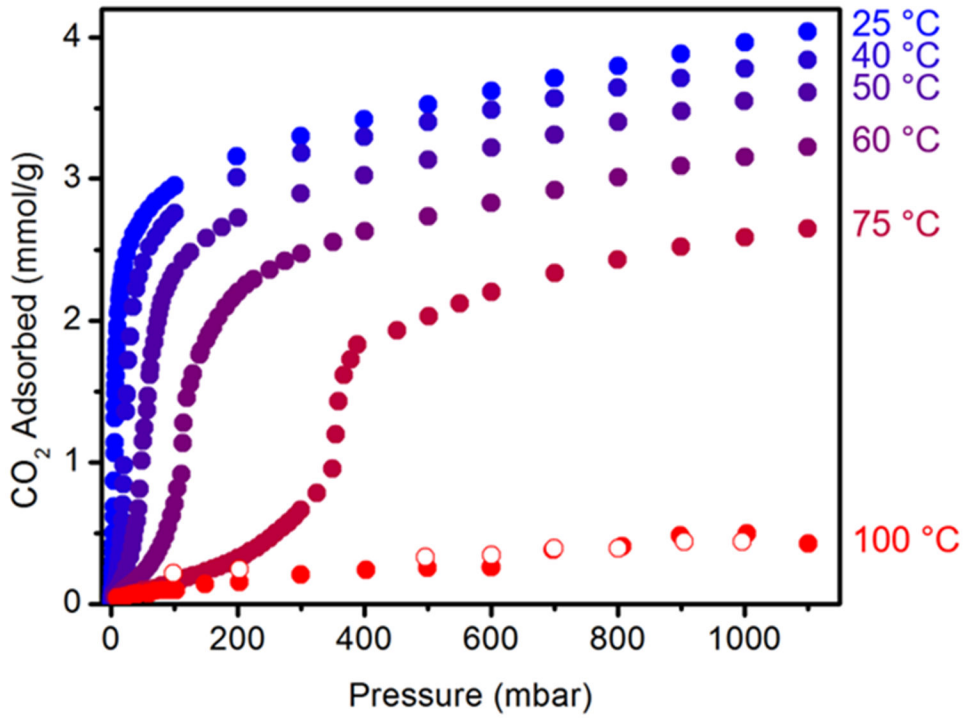

Figure 4.

Isotherms for the adsorption of CO_2 at 25, 40, 50, 60, 75, and 100 °C in dmpn–Mg_2(dobpdc) (desorption data at 100 °C shown with open circles).

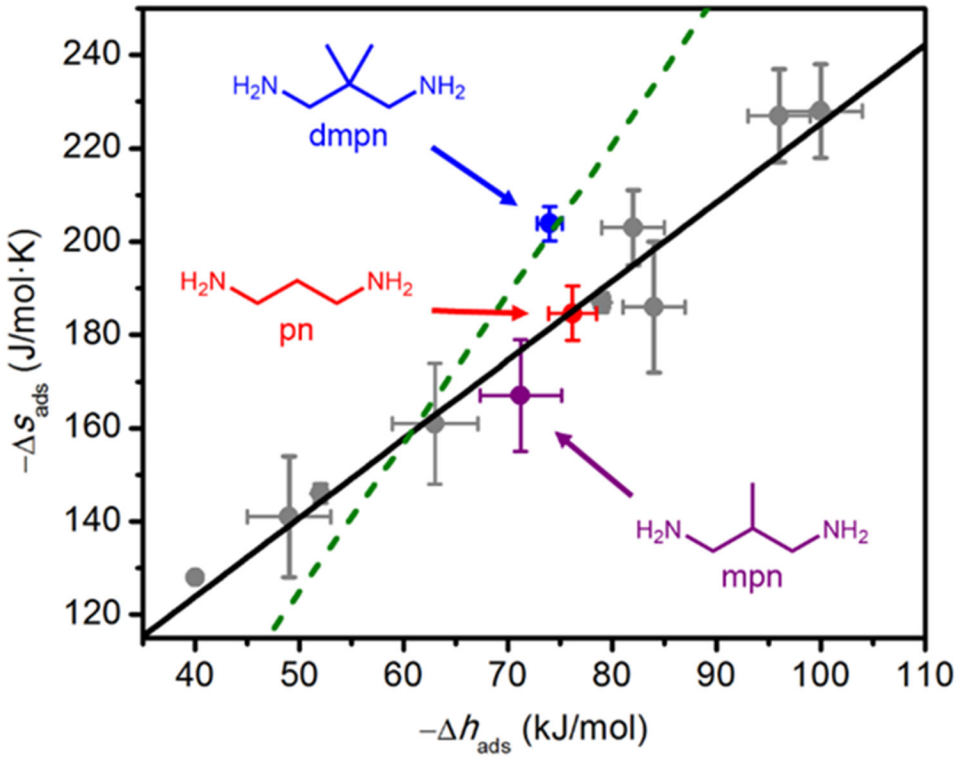

Figure 5.

Correlation between the negative differential enthalpy ($-\Delta h_{ads}$) and negative differential entropy ($-\Delta s_{ads}$) of CO_2 adsorption in diamine-appended variants of Mg_2(dobpdc). The adsorbents mpn–Mg_2(dobpdc) (purple circle), pn–Mg_2(dobpdc) (red circle), and previously reported ethylenediamine-appended variants (gray circles)[16a,17a] follow a linear relationship, whereas dmpn–Mg_2(dobpdc) (blue circle) is an outlier. The dashed green line indicates the combinations of Δh_{ads} and Δs_{ads} that yield Δg_{ads} = −10.9 kJ/mol, corresponding to p_{step} = 15 mbar at 40 °C and thus enabling a 90% capture rate from a coal flue gas stream.

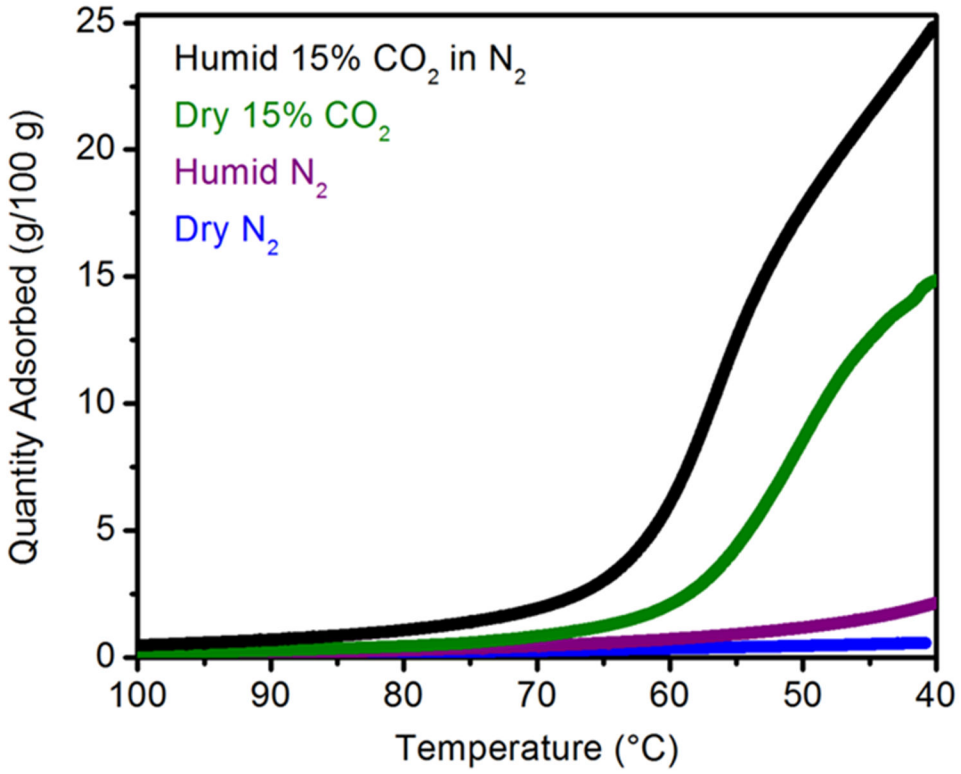

Figure 6.

Humid 15% CO_2 in N_2 (black), dry 15% CO_2 in N_2 (green), humid N_2 (purple), and dry N_2 (dark blue) isobars for dmpn–Mg_2(dobpdc), as determined by thermogravimetric analysis (TGA).

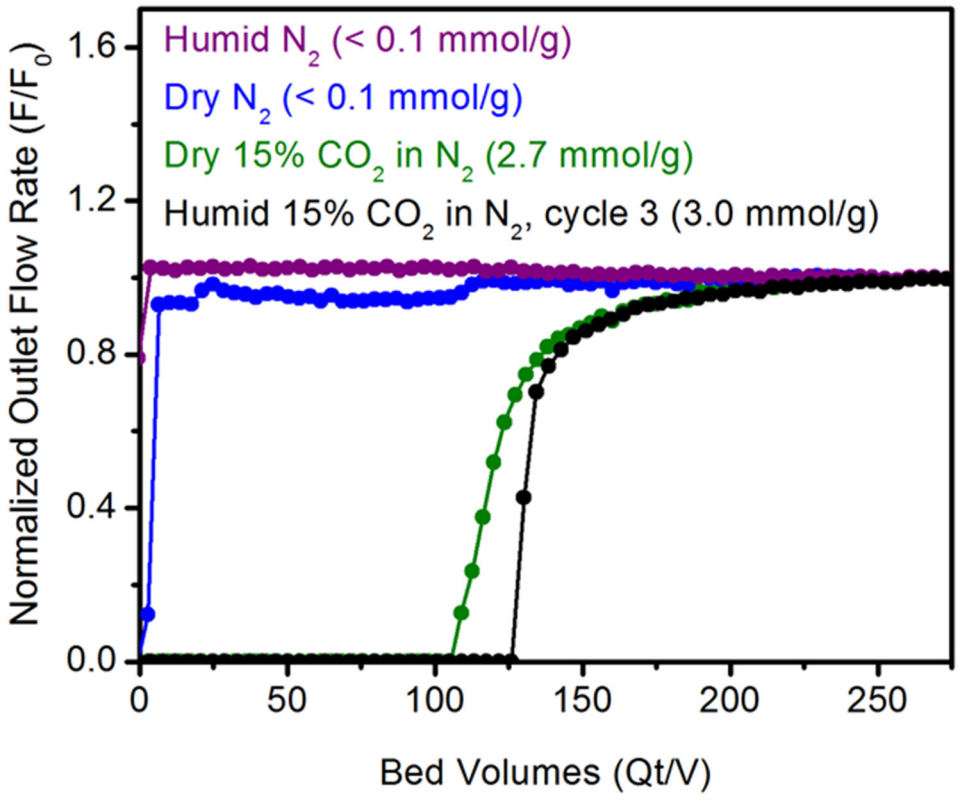

Figure 7.

Dry and humid 15% CO_2 in N_2 breakthrough measurements with dmpn–Mg_2(dobpdc). Breakthrough of N_2 under dry (blue) and humid (purple) conditions occurred nearly immediately, followed by clean breakthrough of CO_2 under both dry (green) and humid (black) conditions.

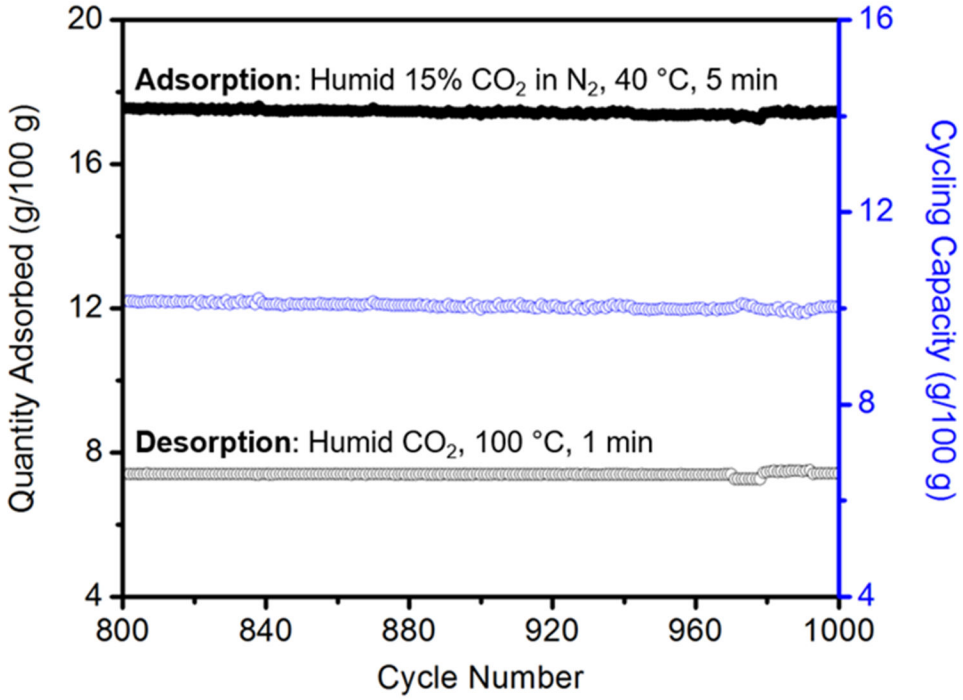

Figure 8.

The adsorption maxima (filled black circles), desorption minima (open black circles), and cycling capacities (open blue circles) of the last 200 of 1000 humid cycles of dmpn–Mg_2(dobpdc), as determined by thermogravimetric analysis (TGA). The baseline value of 0 g/100 g is defined as the mass after activation under humid 15% CO_2 in N_2 for 20 min at 130 °C prior to the first cycle.

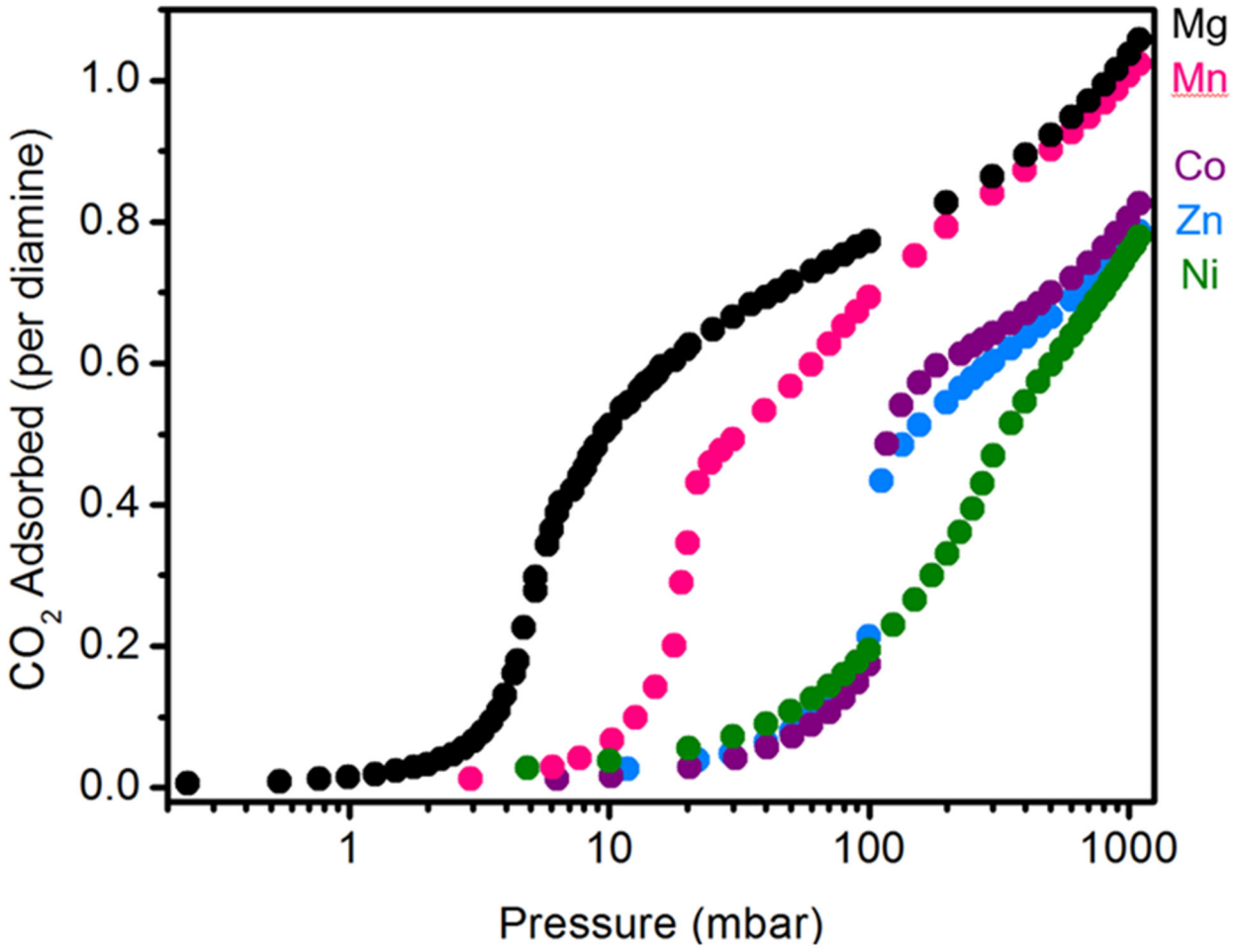

Figure 9.
Metal effect on CO_2 adsorption at 25 °C for dmpn–M_2(dobpdc) (M = Mg, Mn, Co, Zn, Ni).

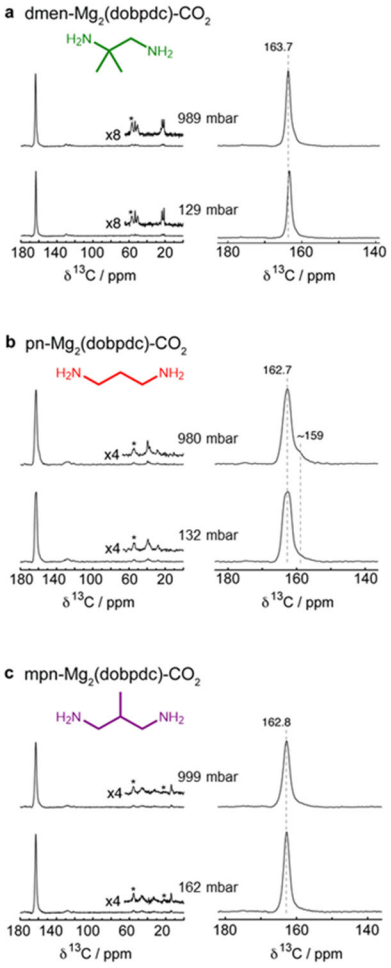

Figure 10.

Room temperature ^{13}C MAS NMR (7.1 T) spectra for (a) dmen–Mg_2(dobpdc), (b) pn–Mg_2(dobpdc), and (c) mpn–Mg_2(dobpdc) dosed with two different pressures of $^{13}CO_2$. Spectra were acquired by cross polarization from ^{1}H. Sample spinning rates were 8 kHz in all cases.

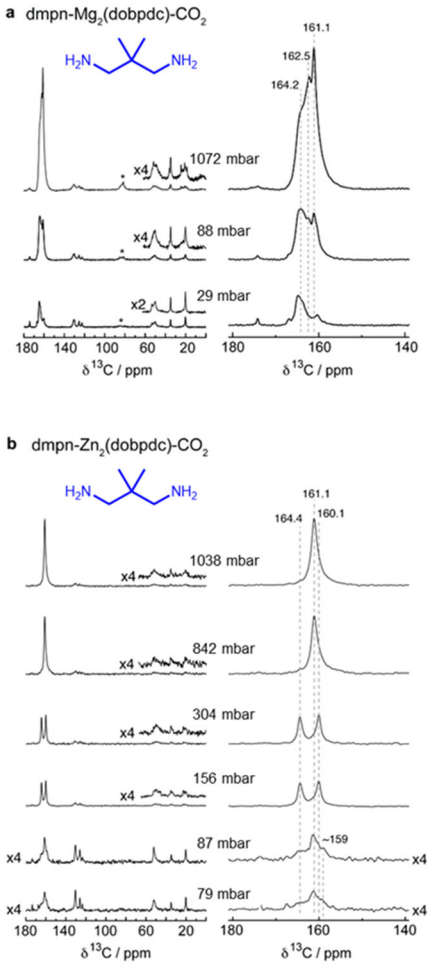

Figure 11.

Room temperature ^{13}C MAS NMR (7.1 T) spectra for (a) dmpn–Mg_2(dobpdc) and (b) dmpn–Zn_2(dobpdc) dosed with various pressures of $^{13}CO_2$. Spectra were acquired by cross polarization from ^{1}H. Sample spinning rates were 8 kHz for dmpn–Mg_2(dobpdc) (a), and 7, 10, 11, 10, 10, 11 kHz for spectra at 79, 87, 156, 304, 842, 1038 mbar, respectively, for dmpn–Zn_2(dobpdc) (b).

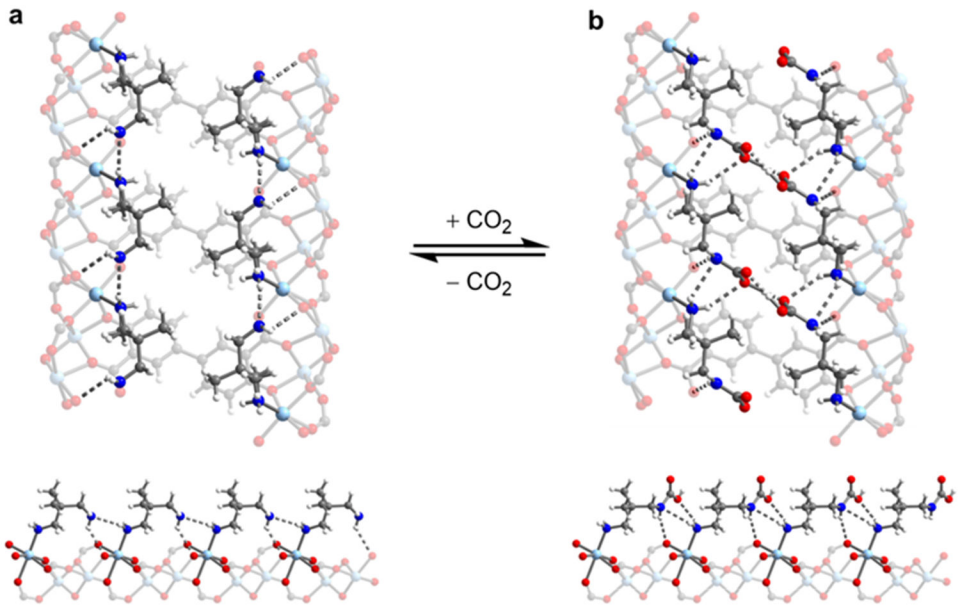

Figure 12.

Single-crystal X-ray diffraction structures of dmpn–Zn_2(dobpdc) at 100 K, with two views shown. a) The structure of diethyl ether-solvated dmpn–Zn_2(dobpdc) shows hydrogen-bonding between adjacent diamines (N···N distance = 3.26(3) Å). b) After activation and dosing with 1 bar of CO_2, dmpn–Zn_2(dobpdc) forms bridging carbamic acid pairs. Extensive hydrogen-bonding of carbamic acids to the framework and between adjacent carbamic acid pairs is observed. The hydrogen atoms between the carbamic acid pairs could not be located crystallographically and are shown here as visual aids.

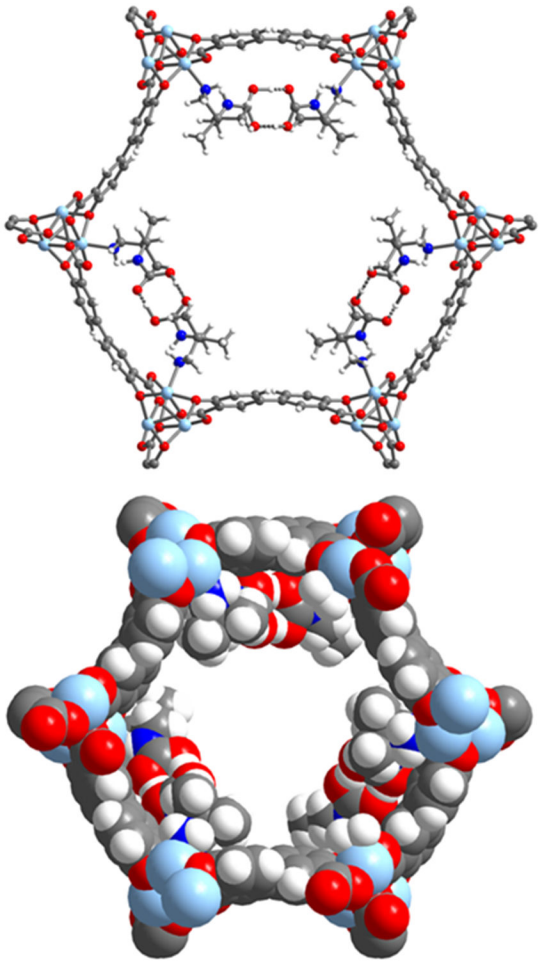

Figure 13.

View down the *c*-axis of the single-crystal X-ray diffraction structure of the carbamic acid pairs formed upon CO_2 adsorption in dmpn–Zn_2(dobpdc) at 100 K. The hydrogen atoms between the carbamic acid pairs could not be located crystallographically and are shown here as visual aids.